Simposio CEA de Robótica, Bioingeniería, Visión por Computador y Automática Marina 2026

Towards Vision-Based Bending Control of a Soft Pneumatic Actuator

Serrano-Balbontín, A.J.[a], Tejado, I.[a,*], Vinagre, B.M.[a], Aphale, S.S.[b], San-Millan, A.[b]

[a] *Escuela de Ingenierías Industriales, Universidad de Extremadura, 06006 Badajoz, Spain.*
[b] *Artificial Intelligence, Robotics and Mechatronic Systems Group (ARMS), School of Engineering, University of Aberdeen, Aberdeen AB24 3UE, U.K.*

Resumen

Los actuadores neumáticos blandos presentan fuertes no linealidades que dificultan el control preciso de su movimiento. En trabajos previos se ha demostrado que la regulación de presión mediante modulación de frecuencia de pulso por integral inversa (IIPFM, por sus siglas en inglés) mejora significativamente el desempeño del lazo interno de control. Este trabajo aborda el control de flexión de un sistema neumático blando, centrándose en el desarrollo del lazo externo de control. Como resultado preliminar, se presenta un algoritmo basado en visión artificial que permite la estimación en tiempo real de la curvatura y la posición del extremo del actuador, habilitando el cierre del lazo externo en desarrollos futuros.

Palabras clave: Tecnología robótica, Control basado en eventos, Algoritmos en tiempo real, programación y planificación.

Towards bending control of a soft pneumatic system: preliminary results

Abstract

Soft pneumatic actuators exhibit strong nonlinearities that hinder precise motion control. Previous work has shown that pressure regulation based on inverse integral pulse frequency modulation (IIPFM) significantly improves the performance of the inner control loop. This paper addresses the bending control of a soft pneumatic system, focusing on the development of the outer control loop. As a preliminary result, a vision-based algorithm is presented to enable real-time estimation of actuator curvature and tip position, providing the basis for closing the outer loop in future developments.

Keywords: Robotics technology, Event-based control, Real-time algorithms, scheduling, and programming.

1. Introduction

Soft pneumatic actuators (SPAs) have gained increasing attention due to their intrinsic compliance, lightweight structure, and suitability for safe interaction in uncertain environments (Gong et al., 2025). These properties make them attractive for soft robotics, bio-inspired systems, and human–robot interaction (Asbeck et al., 2015). However, SPA behaviour is strongly nonlinear and often exhibits hysteresis and time-varying dynamics, which complicates both modelling and control (Wang et al., 2017).

Hierarchical control architectures are commonly adopted, where an inner loop regulates internal pressure and an outer loop controls deformation variables such as curvature or tip position (Zou et al., 2024). While pressure regulation has been widely studied, practical outer-loop implementation is frequently limited by deformation sensing. Several vision-based approaches have been proposed to estimate bending or pose in soft pneumatic systems, including RGB-D sensor fusion for head positioning (Ogunmolu et al., 2016), embedded camera-based proprioception (Zhang et al., 2026; Huang et al., 2025), and deep-learning-based joint angle estimation (Ghobadi et al., 2025). Although these methods demonstrate the potential of vision-based sensing, many rely on specialised hardware, learning-based pipelines, or application-specific configurations, and simple, minimally intrusive solutions for real-time bending estimation remain desirable.

This paper presents preliminary results towards vision-based bending control of a soft pneumatic actuator. A computer-vision algorithm is developed to estimate actuator curvature, bending angle and tip position, providing the sensing layer required to close the outer loop. The proposed approach is conceived to operate on top of an inner pressure regulation layer based on inverse integral pulse frequency modula-

*Autor para correspondencia: itejbal@unex.es

tion (IIPFM), previously validated in (Serrano-Balbontín et al., 2025; Serrano-Balbontín et al., 2026). Overall, the contribution aims to provide a practical and non-intrusive sensing alternative for hierarchical control of SPAs.

The remainder of the paper is organised as follows. Section 2 describes the experimental platform. Section 3 presents the control architecture and the proposed vision-based tracking algorithm. Section 4 reports preliminary experimental results. Finally, Section 5 concludes the paper.

2. Soft pneumatic system

Figure 1 illustrates the soft pneumatic system considered in this work, including the experimental setup and the actuator. The SPA is a dual-cavity pleated structure ($119 \times 37 \times 18$ mm) fabricated from Dragon Skin 20 and designed for dexterous manipulation tasks (Kassim et al., 2023). It is driven by a 3/2 solenoid valve that alternates between pressurising the actuator and venting it to atmosphere. Pressure sensors located at the inlet and outlet provide feedback to the controller, which determines the valve switching in real time. When pressurised, the SPA bends inwards, opposite to the external bellows.

The pneumatic supply chain comprises a compressor, a pressure regulator to maintain a constant supply level, and a 2-litre air tank to mitigate pressure fluctuations and transient demand peaks. The control architecture consists of a PC running MATLAB, a real-time dSPACE platform for control execution and data acquisition, and a driver stage that adapts logic-level commands to the nominal actuation voltage of the valve. A Canon EOS M50 camera is positioned in front of the actuator to capture its deformation, enabling the estimation of bending angle, curvature, and tip displacement during the experiments.

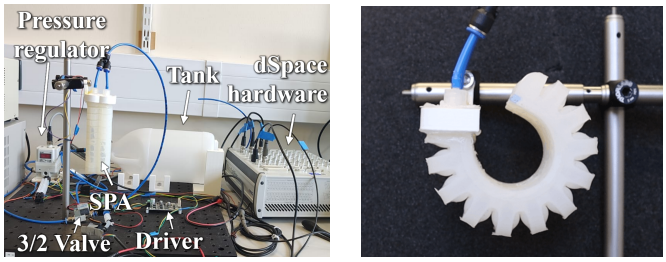

(a) (b)

Figure 1: Soft pneumatic system: (a) experimental setup; (b) actuator under pressurisation.

The pressure dynamics of the SPA are described by a hybrid four-state model. States 1 and 2 represent the discharging and charging phases, respectively, under ideal valve operation. Their dynamics are given by

$$\dot{P}_1(t) = \frac{-\sqrt{P(t)}}{c_1}, \tag{1}$$

$$\dot{P}_2(t) = \frac{-P(t)}{\tau_2} + \frac{k_2}{\tau_2}, \tag{2}$$

where $P(t)$ denotes the actuator pressure, $c_1 = 0.533$ s/bar$^{0.5}$ characterises the discharging process, $\tau_2 = 0.826$ s is the charging time constant, and $k_2 = 0.837$ bar corresponds to the supply pressure.

States 3 and 4 account for the finite valve switching times, denoted t_{on} and t_{off}. During these intervals, the pressure is assumed constant,

$$\dot{P}_{3,t_{on}} = \dot{P}_{4,t_{off}} = 0, \tag{3}$$

with identified values $t_{on} = 3$ ms and $t_{off} = 10$ ms. Further details on the identification procedure are reported in (Serrano-Balbontín et al., 2025).

Due to these switching constraints, the system exhibits a dead-zone when the high-state pulse duration is shorter than t_{on}, and saturation when the low-state duration is shorter than t_{off}.

3. Control of the system

A hierarchical control architecture is adopted for the soft pneumatic system, as shown in Figure 2. A fast inner loop regulates the actuator pressure, while an outer loop addresses deformation objectives such as curvature or tip position. The outer loop generates the pressure reference required to achieve the desired bending, whereas the inner loop ensures accurate pressure tracking. This separation of time scales allows pressure and deformation dynamics to be treated independently, simplifying the overall design.

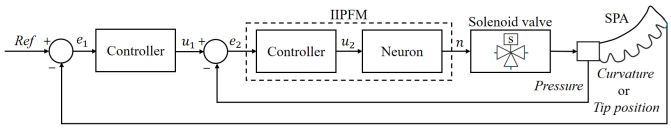

Figure 2: Closed-loop control scheme of the SPA.

3.1. Pressure control: IIPFM

The inner loop regulates the internal SPA pressure using a spiking control strategy based on IIPFM. The method combines a proportional–integral (PI) controller with a neuron-inspired pulse modulator that converts the continuous control signal into a two-state command for the on/off solenoid valve.

IIPFM explicitly accounts for the valve switching constraints by enforcing minimum on- and off-times, thereby mitigating dead-zone and saturation effects. Unlike conventional spiking control, IIPFM integrates the PI controller output $u(t)$, in the form of $A - u(t)$, until a threshold K_{ti} is reached, at which point it emits a pulse of amplitude A and width t_h, and resets the integrator.

In this formulation, the relevant parameter of the output pulse train signal is the low-state duration t_l (constant), whose relationship with the high-state duration is given by:

$$t_h(\xi) = t_l\left(\frac{G}{1-\xi} - 1\right), \tag{4}$$

where ξ denotes the input normalised with respect to the amplitude ($\xi = u/A$) and G is the neuron gain.

By appropriate tuning of the neuron parameters—namely, the pulse amplitude A, the low-sate duration t_l, and the gain G (with the threshold typically defined as $K_{ti} = GAt_l$)—, the combined behaviour of the neuron, valve, and actuator can be approximated by a first-order linear system over a broad operating range. A two-step procedure is followed to tune the neuron

parameters. First, A is fixed according to the nominal valve actuation voltage. Then, t_l is selected to maximise the linearity of both the static and dynamic pressure responses, while satisfying the physical constraints imposed by the valve switching times. Once the neuron is configured, a the PI controller is designed using standard techniques based on the resulting equivalent first-order model. The detailed formulation and tuning procedure of the IIPFM-based controller were previously reported in (Serrano-Balbontín et al., 2026; Serrano-Balbontín et al., 2025).

3.2. Bending control: vision-based tracking algorithm

The outer loop aims at regulating the deformation of the actuator, expressed in terms of curvature or tip displacement. As no embedded deformation sensors are available in the current configuration, a vision-based algorithm has been developed to extract these quantities directly from image sequences. The estimated deformation variables are subsequently used to generate the pressure reference supplied to the inner regulation loop described in Section 3.1.

An overview of the processing stages is depicted in Figure 3. The algorithm was implemented in Python 3.11.9 using the OpenCV 4.12.0 library, and the source code is publicly accessible in (Serrano-Balbontin et al., 2026). The complete pipeline consists of successive segmentation and geometric reconstruction steps, detailed below together with representative intermediate outputs.

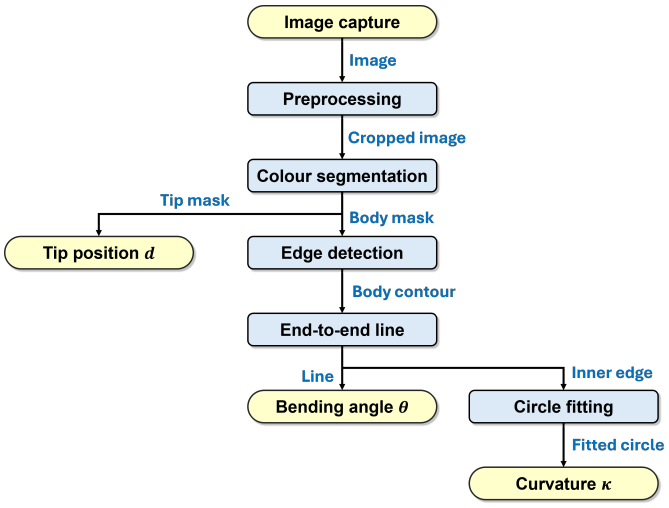

Figure 3: Overview of the vision-based tracking algorithm for SPA bending measurement. Starting from preprocessed frames, the SPA body and tip marker are segmented, the SPA edge and end-to-end line are extracted, and a circular fit yields the curvature (κ), bending angle (θ), and tip displacement (d) at each time instant.

Image acquisition. The actuator is positioned against a dark background to simplify segmentation. The camera optical axis is aligned orthogonally to the plane of bending to minimise perspective distortion. Images are captured at 25 fps with a resolution of 1920×1080 px (full HD). A representative raw frame is shown in Figure 4(a).

Preprocessing. Each frame is initially cropped to isolate the region of interest and eliminate irrelevant background areas, thereby reducing computational load. The resulting image (Figure 4(b)) has a resolution of 500×550 px, corresponding to an approximate 87% reduction in image area. Colour correction is then applied by adjusting gamma, brightness, contrast, saturation, and hue to enhance visual contrast between the actuator and the background. A luma-key operation is additionally performed to map low-luminance pixels to pure black, mitigating the effects of noise and reflections prior to segmentation.

Colour segmentation. The SPA body and a blue marker located at the actuator tip are segmented through colour thresholding in the HSV colour space. Thresholds are independently defined for hue, saturation, and value channels. The outcome of this stage is a binary mask, represented as a matrix matching the cropped image dimensions, where foreground pixels are assigned value 1 and background pixels value 0. Two masks are obtained: one corresponding to the tip marker and another corresponding to the complete actuator body (Figures 4(c) and 4(d)).

Edge detection. The external contour of the segmented actuator body is extracted and used for geometric reconstruction (Figure 4(e)). Contour detection is performed using the Suzuki–Abe algorithm (Suzuki et al., 1985), as implemented in OpenCV. No contour simplification is applied, ensuring an accurate representation of the actuator boundary.

End-to-end line estimation. To characterise the bending configuration, a line segment is defined between the clamped base of the actuator and a second point located along the extracted contour (Figure 4(f)). The base point is fixed throughout the experiment. The second point is obtained as the intersection between the actuator contour and a ray originating from the base. The search begins with a vertical ray and progressively decreases its angle until an intersection with the contour is detected. This iterative procedure ensures robustness even in the absence of a clearly defined tip or when the actuator exhibits a rounded geometry. The slope of the resulting segment is used to compute the bending angle.

Circle fitting. The contour points enclosed between the endpoints of the end-to-end line are selected for geometric approximation. Although the actuator incorporates bellow structures, the small inter-chamber gaps have negligible influence on its global bending behaviour. Therefore, the deformation can be approximated using a constant-curvature assumption, commonly adopted in soft robotics (Torzini et al., 2026). A least-squares circle fitting algorithm is applied to the selected contour points (Figure 4(g)), providing a consistent geometric representation of the actuator shape.

Output variables. From the reconstructed geometry, three deformation metrics are computed at each time instant:

- Tip displacement d, obtained from the centroid of the segmented tip marker.
- Bending angle θ, defined as the angle between the end-to-end line and the vertical reference corresponding to the undeformed configuration.
- Curvature κ, calculated as the inverse of the fitted circle radius ($\kappa = 1/r$).

These quantities provide complementary descriptions of the actuator deformation and can independently serve as controlled variables in the outer loop.

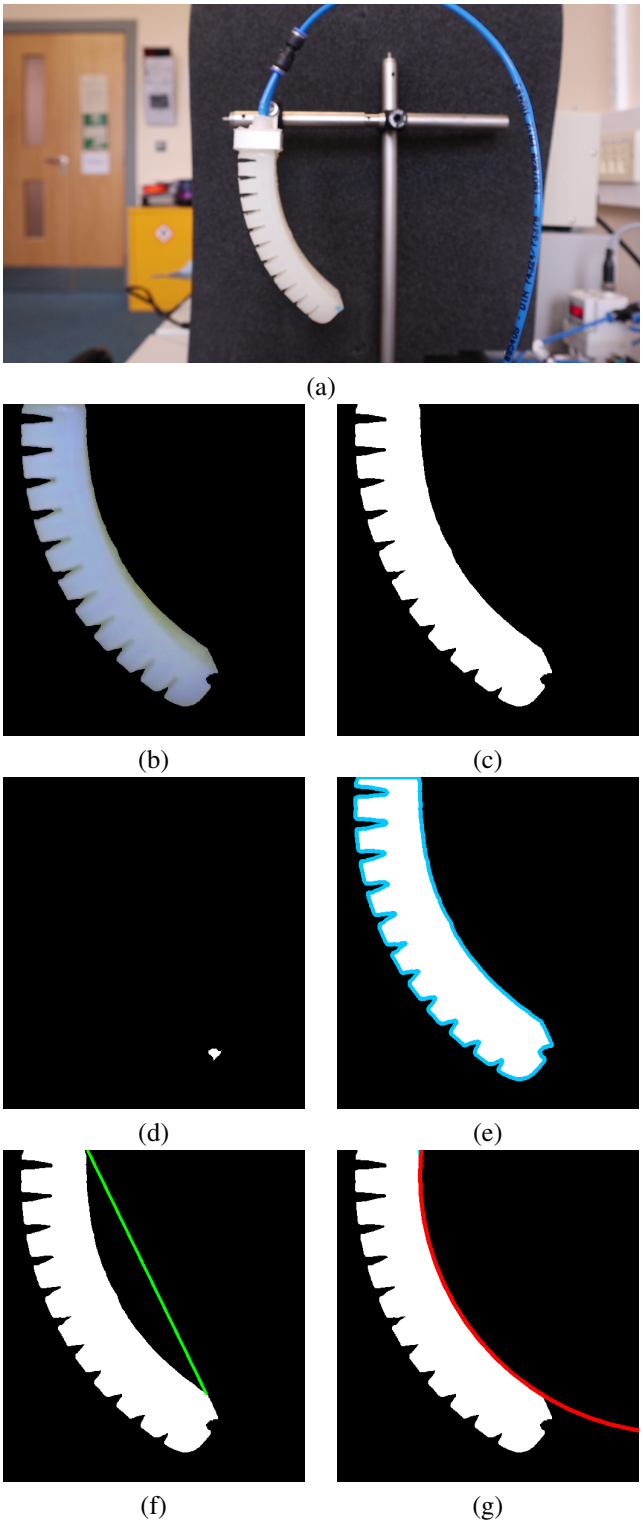

Figure 4: Vision-based tracking algorithm: (a) original image captured by the camera; (b) SPA body; (c) body mask; (d) tip marker of the body mask; (e) body contour (blue) drawn on top of the body mask; (f) end-to-end line (green) drawn on top of the body mask; (g) fitted circle superimposed in red on the body mask.

The proposed approach enables simultaneous estimation of curvature and tip position without physical contact or additional sensing hardware. This is particularly advantageous for soft pneumatic systems, where embedded sensors may compromise compliance or increase system complexity. To facilitate reuse across different actuator designs, the algorithm is parameterised through adjustable colour thresholds, region-of-interest selection, and specification of the base reference point used for geometric reconstruction.

4. Results

This section presents the experimental results obtained for the soft pneumatic system under free-motion conditions. The experiments correspond to the inner pressure regulation loop, during which image sequences were recorded and processed using the proposed vision-based tracking algorithm to estimate the deformation variables d, θ, and κ.

Since the actuator operated without interaction with external objects, the analysis focuses on the curvature κ as the primary deformation descriptor. Under the constant-curvature assumption, the remaining variables can be geometrically derived from κ.

The actuator outlet pressure was regulated using the IIPFM-based strategy described in Section 3.1, while deformation was recorded simultaneously. The neuron parameters were set to $t_l = 19$ ms, $A = 1$ (normalised logic, scaled to 24 V for valve actuation), and $G = 1.15$, with PI gains $K_p = 0.1$ and $K_i = 0.3$. The effectiveness of the pressure regulation strategy was previously validated in (Serrano-Balbontín et al., 2026).

The recorded video data were processed offline using the algorithm described in Section 3.2. Figure 5 shows the estimated pressure together with the estimated curvature during a multistep experiment. The curvature evolution follows the pressure profile with similar temporal behaviour, confirming the capability of the proposed algorithm to capture the actuator deformation consistently with the internal pressure dynamics.

Nevertheless, the relationship between pressure and curvature is clearly nonlinear, as curvature amplitudes do not scale proportionally with pressure variations. This behaviour is attributed to the viscoelastic characteristics of the soft material and gravitational effects, which introduce load- and rate-dependent phenomena. These observations highlight the need for dedicated outer-loop strategies, which will be addressed in future work.

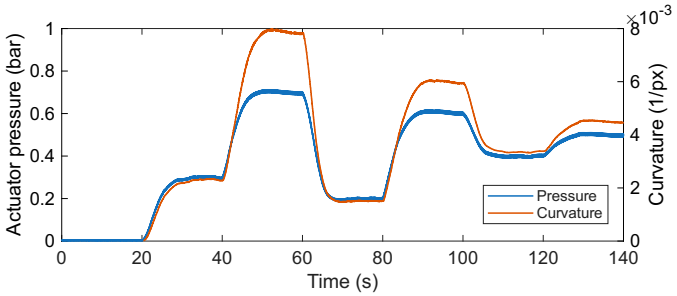

Figure 5: Closed-loop pressure (blue) and the corresponding SPA curvature (red) under IIPFM control for the multistep experiment. Curvature follows the pressure profile with a nonlinear gain, enabling future outer-loop control of shape or tip position once pressure is tightly regulated.

5. Conclusions

This paper has presented preliminary results towards vision-based bending control of a soft pneumatic actuator. A

computer-vision algorithm has been developed to estimate actuator curvature, bending angle, and tip displacement from image sequences, enabling non-intrusive deformation sensing for hierarchical control architectures.

Experimental results obtained under free-motion conditions have shown that the proposed approach provides consistent curvature estimation in agreement with the regulated pressure dynamics of the inner loop. The measurements reveal a nonlinear relationship between pressure and curvature, reflecting the viscoelastic behaviour of the soft material and the influence of gravitational effects.

The presented framework establishes the sensing layer required for closing the outer deformation control loop. Future work will address the identification of pressure–curvature model and the design of dedicated outer-loop control strategies based on the proposed vision-based estimation method.

Agradecimientos

This research was funded by the Agencia Estatal de Investigación (Ministerio de Ciencia e Innovación) through project PID2022-141409OB-C22/AEI/10.13039/501100011033/FEDER, UE, by the Junta de Extremadura through grant GR24059 within "Ayudas a Grupos de Investigación", and by the European Regional Development Fund (FEDER) "A way to make Europe".

Andrés Serrano would like to thank the Ministerio de Ciencia, Innovación y Universidades for its support through the scholarship no. FPU22/00885 of the FPU Program.

References

Asbeck, A. T., Rossi, S. M. D., Holt, K. G., Walsh, C. J., 2015. A biologically inspired soft exosuit for walking assistance. The International Journal of Robotics Research 34 (6), 744–762.
DOI: 10.1177/0278364914562476

Ghobadi, N., Kinsner, W., Szturm, T., Sepehri, N., 2025. Design and evaluation of a soft robotic actuator with non-intrusive vision-based bending measurement. Sensors 25 (13).
DOI: 10.3390/s25133858

Gong, S., Ye, X., Wang, Y., Li, W., Zhang, W., Shao, L., 2025. High-precision control of an antagonistic soft continuum robot for dexterous objects grasping and assembly. Sensors and Actuators A: Physical 391, 116669.
DOI: 10.1016/j.sna.2025.116669

Huang, T., Ren, J., Yang, X., Wu, L., Zhang, J., Zhang, N., Gu, G., 2025. Intrinsic vision-based learning for proprioceptive sensing of soft pneumatic actuators. In: Proceedings of the 18th International Conference on Intelligent Robotics and Applications (ICIRA 2025) Okayama, Japan, August 6–9. Springer-Verlag, Berlin, Heidelberg, p. 65–76.
DOI: 10.1007/978-981-95-2095-4_6

Kassim, S. O., Visnevskis, K., Vaziri, V., Aphale, S. S., 2023. A dual cavity pleated structures soft pneumatic actuator for soft robotic applications. In: 2023 IEEE AFRICON. pp. 1–6.
DOI: 10.1109/AFRICON55910.2023.10293725

Ogunmolu, O. P., Gu, X., Jiang, S., Gans, N. R., 2016. Vision-based control of a soft robot for maskless head and neck cancer radiotherapy. In: Proceedings of the 2016 IEEE International Conference on Automation Science and Engineering (CASE). pp. 180–187.
DOI: 10.1109/COASE.2016.7743378

Serrano-Balbontin, A. J., Tejado, I., Vinagre, B. M., 2026. SoftBendingCV: Bending Measurements of Soft Actuators using Computer Vision.
URL: https://github.com/ajserranob/SoftBendingCV.git

Serrano-Balbontín, A. J., Tejado, I., Vinagre, B. M., Aphale, S. S., San-Millan, A., 2025. Open-loop characterisation of soft actuator pressure regulated by pulse-driven solenoid valve. Robotics 14 (12).
DOI: 10.3390/robotics14120177

Serrano-Balbontín, A. J., Tejado, I., Vinagre, B. M., Aphale, S. S., San-Millan, A., 2026. Spiking control of a solenoid valve for high-precision pressure regulation in soft robotics. IEEE Control Systems Letters 10, 127–132.
DOI: 10.1109/LCSYS.2026.3672133

Suzuki, S., et al., 1985. Topological structural analysis of digitized binary images by border following. Computer Vision, Graphics, and Image Processing 30 (1), 32–46.

Torzini, L., Puggelli, L., Governi, L., Buonamici, F., Furferi, R., Volpe, Y., 2026. 3D-printed soft pneumatic actuators: Influence of geometric design and operating conditions on bending angle and force output. Journal of Advanced Manufacturing Science and Technology 6 (1), 2026004.
DOI: 10.51393/j.jamst.2026004

Wang, H., Yang, B., Liu, Y., Chen, W., Liang, X., Pfeifer, R., 2017. Visual servoing of soft robot manipulator in constrained environments with an adaptive controller. IEEE/ASME Transactions on Mechatronics 22 (1), 41–50.
DOI: 10.1109/TMECH.2016.2613410

Zhang, R., Yoo, U., Li, Y., Agarwal, A., Yuan, W., 2026. Pneugelsight: Soft robotic vision-based proprioception and tactile sensing.
DOI: 10.48550/arXiv.2508.18443

Zou, S., Picella, S., de Vries, J., Kortman, V. G., Sakes, A., Overvelde, J. T. B., Jan 2024. A retrofit sensing strategy for soft fluidic robots. Nature Communications 15 (1), 539.
DOI: 10.1038/s41467-023-44517-z